HIGH ACCURACY TRACKING OF TARGETS USING MASSIVE MIMO

Xiaolu Zeng[*], *Feng Zhang*[*†], *Beibei Wang*[*†] *and K. J. Ray Liu*[*†]

[*]University of Marland, College Park, MD 20742, USA.
[†] Origin Wireless Inc., 7500 Greenway Center Drive, Suite 1070, MD 20770, USA.

ABSTRACT

While high accuracy tracking of targets has been extensively explored because of its wide applications, many exiting methods degenerate in the presence of multipath distortions. This paper proposes an accurate and novel multipath-resilient system to track the targets by leveraging the large number of antennas in massive MIMO systems. We first prove that statistical autocorrelation of the received energy physically shows a sinc-like distribution around the receiver in far-field scenario. Based on such an observation, a novel method is developed to estimate the moving speed of the target with respect to a single base station. The absolute moving speed and direction are further estimated by using the geometrical relationships among multiple base stations and thus we can track the target by dead-reckoning using the consecutive moving speed and moving direction estimations. Numerical simulations show that the proposed system can achieve decimeter-lever accuracy for tracking in various environments, which outperforms the existing methods.

Index Terms— target tracking, massive MIMO, decimeter-level accuracy, multipath-resilient

1. INTRODUCTION

Target tracking plays an important role in modern life with wide applications in autonomous driving and navigation systems. Although the global positioning system (GPS) [1] can achieve good accuracy for the real-time tracking of outdoor targets, it requires an unobstructed line-of-sight (LOS) path to at least four GPS satellites. However, its performance degrades seriously when the LOS signal is blocked, especially in urban areas where the LOS signal is often blocked by tall buildings. As a result, it is of great importance to explore a real-time tracking method which can achieve high accuracy while working robustly in both LOS and non-line-of-sight (NLOS) scenarios [2–4].

In principle, tracking methods can be classified into two categories, i.e., triangulation-based methods and fingerprinting-based methods. Triangulation-based methods firstly estimate the direction-of-arrival (DOA) [5–7], time-of-arrival (TOA) [8] with respect to all the stations. Then, triangular relationships among multiple stations are leveraged to estimate the location of the target and subsequently track the target timely. Fingerprinting-based methods first construct an offline database of positions together with corresponding signatures such as received signal strength (RSS) [9] and channel state information (CSI) [10, 11] in the area of interest. Then, the online signatures are measured and matched with the offline database to estimate the location of the target. However, triangulation-based methods degenerate significantly in the presence of multipath/NLOS signals since only LOS signal is useful for DOA/TOA estimations. Fingerprinting-based methods usually suffer from a prohibitive overhead to construct and update the offline database especially in dynamic environments.

Different from the existing methods, this paper develops a high accuracy tracking system by exploring the statistical property, i.e., autocorrelation function (ACFS) of the received signal in massive MIMO systems [12–14]. The ACFS is proved to be a stable sinc-like focusing beam around the receiver in which the stability comes from the fact that the received signal in massive MIMO system contains a large number of LOS and NLOS signal components. Based on the ACFS, we then develops an algorithm to estimate the moving speed and direction of the target and thus can track a target timely. The proposed tracking system is multipath-resilient because the ACFS is stable regardless of the environments. In addition, it also enjoys a low complexity because we only need to compute the ACFS of the received signal while it is very straightforward to calculate the location of the target by using the derived close-form expressions. The system can support massive concurrent targets/clients without affecting the channel capacity since a target/client only listens to the BSs. Extensive simulation results demonstrate that the proposed system can track a target with decimeter-level accuracy, which shows superiority than the benchmark algorithms.

The rest of the paper is organized as follows. We first present the signal model followed by the focusing beam derivation in Section 2. Section 3 introduces the speed estimation and tracking method. System performance is evaluated by numerical simulations in Section 4. Finally, Section 5 concludes the paper.

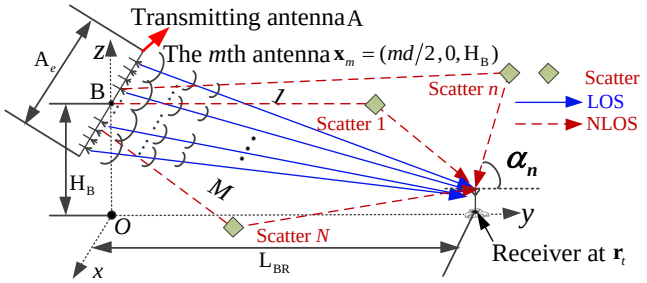

Fig. 1: 3-dimensional signal propagation geometry.

2. SIGNAL MODEL AND FOCUS BEAM IN MASSIVE MIMO

This section first introduces the signal model and then derives ACFS of the received signal, whose distribution exhibits a focusing beam around the receiver in massive MIMO systems.

2.1. Signal Model

As shown in Fig. 1, a receiver fixed on a mobile object receives the signal coming from a base station (BS) with M antennas. 'B' and $\mathbf{r}_t$ represents the center of the base station and receiver location at time t respectively. $\mathrm{H_B}$ and $\mathrm{L_{BR}}$ denote the altitude of the BS and the horizontal distance between the BS and the receiver. A_e is the aperture of the antenna A. Then, the received signal consisting of LOS and NLOS signal components can be expressed as [15–17]

$$\begin{aligned} y(t) &= y_{\mathrm{L}}(t) + y_{\mathrm{N}}(t) + n(t), \\ y_{\mathrm{L}}(t) &= \sqrt{K_{\mathrm{L}}} \sum_{m=1}^{M} \frac{\exp(j(k|\mathbf{x}_m\mathbf{r}_t| + \phi_m))}{4\pi|\mathbf{x}_m\mathbf{r}_t|}, \\ y_{\mathrm{N}}(t) &= \sqrt{K_{\mathrm{N}}} \sum_{n=1}^{N} \exp[j(\omega_d t \cos\alpha_n + \phi_n)], \end{aligned} \tag{1}$$

where $y_{\mathrm{L}}(t)$ and $y_{\mathrm{N}}(t)$ represent LOS and NLOS component with power coefficient K_{L} and K_{N}. $k = 2\pi/\lambda$ denotes the wave number where λ is the wave length. ω_d is the maximum Doppler frequency. $\mathbf{x}_m$ and $\mathbf{r}_t$ are the coordinates of the m-th antenna and the receiver at time t, respectively, $|\mathbf{x}_m\mathbf{r}_t|$ denotes the distance between $\mathbf{x}_m$ and $\mathbf{r}_t$. $n(t)$ is the additive Gaussian noise while ϕ_m is the phase distortion of the m-th LOS signal. α_n and ϕ_n are the DOA and phase distortion of the n-th NLOS signal component. In general, ϕ_m, α_n, and ϕ_n can be assumed as i.i.d uniformly distributed over $[-\pi, \pi)$ [18]. In far-filed scenario where $\mathrm{L_{BR}} \geq 10\mathrm{H_B} \gg \mathrm{A}_e$ holds, the 3-dimensional signal propagation geometry in Fig. 1 can be simplified as a 2-dimensional version shown in Fig. 2 in which we omit the NLOS signals since their DOAs are assumed to be uniform distributed over $[-\pi, \pi)$. $\mathbf{r}_0$ and $\mathbf{r}_s$ represents the location of the target at t_0 and t_s while $L = \sqrt{L_{\mathrm{BR}}^2 + H_{\mathrm{B}}^2}$.

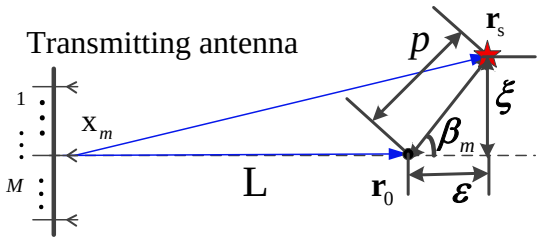

Fig. 2: 2-dimensional signal propagation geometry.

2.2. Focusing Beam Derivation

In this part, we derive the ACF of the received signal which shows a stable distribution in spatial domain around the receiver and thus can be used for target tracking. Recalling (1), the ACF of the received signal can be expressed as

$$\eta_y(\mathbf{r}_0, \mathbf{r}_s) = \mathbb{E}[y(t_0)y^*(t_s)] \approx \eta_{y_{\mathrm{L}}} + \eta_{y_{\mathrm{N}}} + \eta_{\mathrm{n}}, \tag{2}$$

where $\eta_{y_{\mathrm{N}}} = K_{\mathrm{N}} N J_0(kp)$ (see [18, 19]). $\mathbb{E}$ represents expectation operator and $J_0(\cdot)$ is the 0-order Bessel function while p denotes the distance between $\mathbf{r}_0$ to $\mathbf{r}_s$ as shown in Fig. 2. Next, the ACF of the LOS signal can be given by

$$\begin{aligned} &\eta_{y_{\mathrm{L}}} = \eta_{y_{\mathrm{L}}}(\mathbf{r}_0, \mathbf{r}_s) = \mathbb{E}[y_{\mathrm{L}}(t_0)y_{\mathrm{L}}^*(t_s)] = K_{\mathrm{L}} \cdot \\ &\sum_{i=1}^{M}\sum_{m=1}^{M} \mathbb{E}_\phi \left\{ \frac{\exp[j(k(|\mathbf{x}_i\mathbf{r}_0| - |\mathbf{x}_m\mathbf{r}_s|) + \phi_i - \phi_m)]}{(4\pi)^2 |\mathbf{x}_i\mathbf{r}_0||\mathbf{x}_m\mathbf{r}_s|} \right\}, \end{aligned} \tag{3}$$

where $\mathbb{E}_\phi$ means expectation over variable ϕ. Given the far-field condition ($\mathrm{L_{BR}} \gg \mathrm{A}_e$), we can assume $|\mathbf{x}_i\mathbf{r}_0| \approx |\mathbf{x}_m\mathbf{r}_s|$ in the denominator of (3). However, similar approximation is not applicable in the numerator of (3) because the phase term in (3) will change 2π whenever $|\mathbf{x}_i\mathbf{r}_0| - |\mathbf{x}_m\mathbf{r}_s|$ changes by $\lambda = 1/f_c$, which is very small for 5G communication system because of the high carrier frequency f_c [20].

Next, we decompose (3) into two different cases, i.e., a) $i = m$ and b) $i \neq m$. When $i = m$, we have

$$\eta_{y_{\mathrm{L}}}^{\mathrm{1st}} = K_{\mathrm{L}} \sum_{m=1}^{M} \exp(jk(|\mathbf{x}_m\mathbf{r}_0| - |\mathbf{x}_m\mathbf{r}_s|)), \tag{4}$$

where

$$\begin{aligned} &\Big||\mathbf{x}_m\mathbf{r}_0| - |\mathbf{x}_m\mathbf{r}_s|\Big| \approx p\cos\beta_m = \frac{-L\boldsymbol{\epsilon} + x_m\boldsymbol{\xi}}{\sqrt{L^2 + x_m^2}} \\ &\approx -\boldsymbol{\epsilon} + x_m\boldsymbol{\xi}/L. \end{aligned} \tag{5}$$

We note that the derivation of (5) takes the far-filed condition that $\mathrm{L_{BR}} \geq 10\mathrm{H_B} \gg \mathrm{A}_e$. Substituting (5) into (3), $\eta_{y_{\mathrm{L}}}^{\mathrm{1st}}$ can be computed as

$$\begin{aligned} \eta_{y_{\mathrm{L}}}^{\mathrm{1st}} &= \exp(jk\boldsymbol{\epsilon}) \sum_{m=1}^{M} \exp(-jkx_m\boldsymbol{\xi}/L) \\ &= \frac{\mathrm{A}_e \exp(jk\boldsymbol{\epsilon})}{d} \mathrm{sinc}\left(\frac{k\boldsymbol{\xi}\mathrm{A}_e}{2L}\right) \end{aligned}, \tag{6}$$

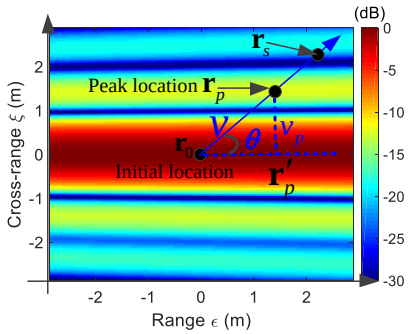

Fig. 3: ACFS of a moving target.

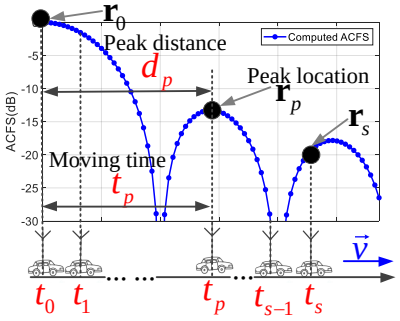

Fig. 4: Speed estimation illustration.

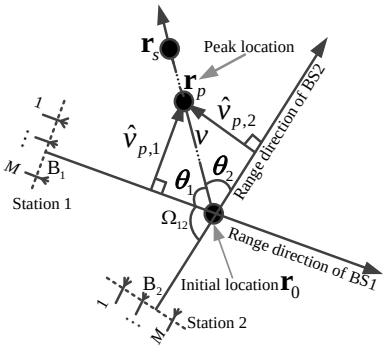

Fig. 5: Two station scenario.

where $\text{sinc}(t) = \sin(t)/t$ is the Sinc function. Next, when $i \neq m$, we have

$$\eta_{y_{\text{L}}}^{\text{2nd}} = K_{\text{L}} \cdot \sum_{i=1}^{M} \sum_{\substack{m=1,\\ m\neq i}}^{M} \mathbb{E}_\phi\{\exp[j(k(|\mathbf{x}_i\mathbf{r}_0| - |\mathbf{x}_m\mathbf{r}_s|) + \phi_i - \phi_m)]\}. \quad (7)$$

The (i, m) pair of (7) is expressed as

$$\begin{aligned}\eta_{y_{\text{L}}}^{\text{2nd}}(i,m) &= \mathbb{E}_\phi\{\exp(\underbrace{\psi_{i,0} - \psi_{m,s}}_{\Psi_{im}} + \underbrace{(\phi_i - \phi_m)}_{\Phi})\} \\ &= \mathbb{E}_\phi\{\cos(\Psi_{im} + \Phi)\} + j\mathbb{E}_\phi\{(\sin(\Psi_{im} + \Phi))\},\end{aligned} \quad (8)$$

where $\psi_{i,0} = k|\mathbf{x}_i\mathbf{r}_0|$, $\psi_{m,s} = k|\mathbf{x}_m\mathbf{r}_s|$. Since ϕ_i and ϕ_m are uniformly distributed over $[-\pi, \pi)$, we have

$$\mathbb{E}_\phi\{\cos(\Psi_{im} + \Phi)\} = 0, \ \mathbb{E}_\phi\{\sin(\Psi_{im} + \Phi)\} = 0. \quad (9)$$

As a result, we have

$$\eta_{y_{\text{L}}}^{\text{2nd}} = K_{\text{L}} \cdot \sum_{i=1}^{M} \sum_{\substack{m=1,\\ m\neq i}}^{M} \eta_{y_{\text{L}}}^{\text{2nd}}(i,m) = 0. \quad (10)$$

Given $\eta_{y_{\text{L}}}^{\text{1st}}$ in (6), $\eta_{y_{\text{L}}}^{\text{2nd}}$ in (10) and $\eta_{y_{\text{N}}} = K_{\text{N}} N J_0(kp)$, the ACF of the received signal can be expressed as

$$\eta_y(\mathbf{r}_0, \mathbf{r}_s) = \quad (11)$$

$$\frac{\text{A}_e \exp(jk\boldsymbol{\epsilon})}{d} \text{sinc}(\frac{k\boldsymbol{\xi}\text{A}_e}{2L}) + K_{\text{N}} N J_0(kp) + \sigma^2\mathbf{I}, \quad (12)$$

where σ^2 is the power spectral density of the noise $\text{n}(t)$. In (12), $K_{\text{N}} N J_0(kp)$ decays much faster than $\text{sinc}(\frac{k\boldsymbol{\xi}\text{A}_e}{2L})$ while σ^2 is a constant. As a result, after normalization and taking the square, we can get the approximation of ACFS, i.e.,

$$|\eta_y(\mathbf{r}_0, \mathbf{r}_s)|^2 = \left|\text{sinc}(\frac{k\boldsymbol{\xi}\text{A}_e}{2L})\right|^2. \quad (13)$$

Note that we omit the proof details which will be given in our future work due to the length limitation of the paper. Simulation in Fig. 3 validates that the ACFS demonstrates a beam pattern around the intended location ($\epsilon = 0, \ \xi = 0$).

3. SPEED ESTIMATION AND TARGET TRACKING

As shown in Fig. 3 , a moving target (from $\mathbf{r}_0$ to $\mathbf{r}_s$) keeps recording signals from the massive MIMO antennas on the BS. Then, the computed ACFS of the measured signal $y(t)$ is a sampled version of the theoretical ACFS $\left|\text{sinc}(\frac{k\boldsymbol{\xi}\text{A}_e}{2L})\right|^2$. As a result, when the target reaches to the first local peak $\mathbf{r}_p$ starting from $\mathbf{r}_0$, the peak distance d_p in Fig. 4 can be estimated by extracting the first local peak of the theoretical ACFS and given by

$$d_p = 2.86L/k\text{A}_e. \quad (14)$$

Similarly, the moving time $\hat{t}_p$ from $\mathbf{r}_0$ to $\mathbf{r}_p$ can be estimated by looking for the first local peak of the computed ACFS of $y(t)$, i.e.,

$$\hat{t}_p = \underset{\tau\in\{0,\Delta t, 2\Delta t, \cdots, T_{\text{ACFS}}\}}{\arg \textbf{FindPeak}} \{|\mathbb{E}[y(t_0)y^*(t_0+\tau)|^2\}, \quad (15)$$

where operation $\textbf{FindPeak}\{\bullet\}$ means looking for the first peak and T_{ACFS} is the time window length within which the first peak may fall in. Given d_p and $\hat{t}_p$, the **projected speed** (see Fig. 3) is estimated by $\hat{v}_p = d_p/\hat{t}_p$.

Consider a practical case where a target can receive signals from Q nearby stations, the **absolute speed** can be given by

$$\begin{cases} v = \dfrac{\hat{v}_{p,q}}{\sin\theta_q}, q = 1, 2, \cdots, Q, \\ \theta_q + \theta_l = 180 - \Omega_{ql}, q \neq l, q, l \in \{1, 2, \cdots, Q\}, \end{cases} \quad (16)$$

where θ_q represents the angle between the moving direction and the line joining the target and center of station q (see Fig. 3). In (16), Ω_{ql} is the angle between $\text{B}_l\mathbf{r}_0$ and $\text{B}_q\mathbf{r}_0$ with vertex $\mathbf{r}_0$ (e.g., $i = 1, q = 2$ in Fig. 5), which is known a priori since the location of the base stations and the initial location are easy to get in communication systems. Fig. 5 gives an example of two base stations, i.e., Q = 2. By solving (16), we can get the moving speed v and also the moving

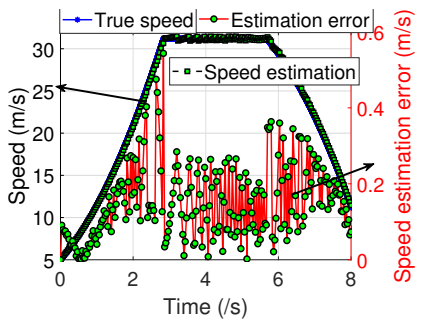

Fig. 6: Speed estimation.

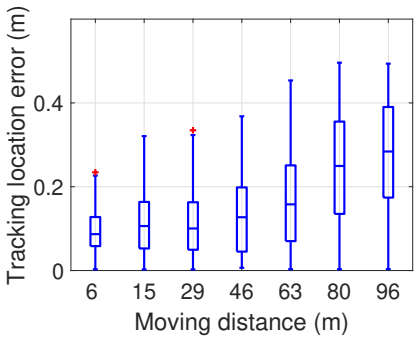

Fig. 7: Tracking location error.

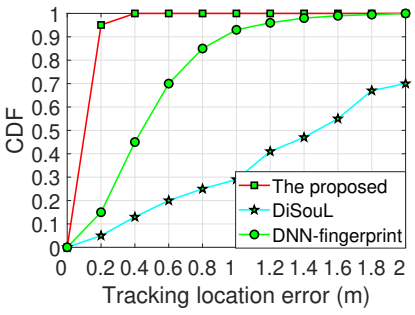

Fig. 8: Performance comparison

direction θ_q estimations simultaneously. Then, the location of the receiver at t_{s+1} can be estimated by

$$\mathbf{r}_{s+1} = \mathbf{r}_s + \Delta\mathbf{r}_s = \mathbf{r}_s + \overrightarrow{\mathbf{v}}\Delta t \tag{17}$$

where Δt is the moving time window during which we assume that moving speed is constant. Note that Δt is flexible with a recommendation of ≤ 0.1s in practice. $\overrightarrow{\mathbf{v}}$ is the velocity vector with module v and direction θ_q. Next, we update $\mathbf{r}_{s+1}$ as the new starting point and repeat the above ACFS computation, moving speed and direction estimation, thus achieve real-time tracking of a moving target.

4. SIMULATION RESULTS

In this section, simulations are conducted to evaluate the performance of the proposed method based on a 5G communication system with carrier frequency $f_c = 28$GHz [20] and antenna number $M = 100$.

4.1. Speed Estimation Results

Fig. 6 shows the speed estimation results during which the targets starts moving at 5m/s. Then it accelerates with a variable acceleration from $t = 0$s to $t = 3$s and moves at a constant speed from $t = 3$s to $t = 5.5$s. Finally, it decelerates with a variable deceleration from $t = 5.5$s to $t = 8$s. In total, it moves about 100m away from the starting point. From Fig. 6, more than 95% speed estimation errors are less than 0.35m/s, which indicates that our method can achieve accurate speed estimations for a practical moving target with different speeds, accelerations and decelerations. Note that it is reasonable for the speed estimation error to fluctuate within a certain extent because the geometrical relationship among the stations and the target varies when the target moves to target locations.

4.2. Performance in Tracking Location Error

To evaluate the location error of the proposed tracking system, we conduct 1000 independent Monte Carlo simulations in which the target moves at variable speeds along a curved trajectory while SNR is fixed at 10dB. Considering the coverage of 5G massive MIMO base stations, the distance between the target and base stations is limited to less than 200m. The number of multipaths is randomly chosen from 10 to 100 in different Monte Carlo trials (driven by the practical measurements in the New York City [21]). Fig. 7 shows the tracking location errors at 10 representative locations of the target on the trajectory. From Fig. 7, the medium error is less than 0.1m when the moving distance is less than 50m while the maximum location error is less than 0.3m, which shows robust decimeter-level tracking accuracy under different NLOS distortions.

Fig. 8 compares the proposed method with the latest triangulation-based DiSouL [12] and DNN-fingerprint [13] methods. As depicted in Fig. 8, the 90 percentile error of our method is 0.18m and DNN-fingerprint demonstrates a 1.2m estimation error. DiSouL cannot achieve less than 2m estimation errors of 90 percentile. Overall, our method is more robust and outperforms the benchmark DiSouL and DNN-fingerprint methods. This is mainly because of the stable statistical distribution of the ACFS of the received signal in a 5G massive MIMO system, while DiSouL relies on two environment-sensitive hyper-parameters in the sparse signal model and the offline database in DNN-fingerprint is vulnerable to dynamic environments.

5. CONCLUSION

This paper presents a novel target tracking method in a 5G massive MIMO system. We prove that the ACFS of the received signal in a massive MIMO system shows a sinc-like focusing beam around the receiver in spatial domain. By considering the geometrical relationship between multiple stations and the target, a speed estimation and tracking algorithm is developed. Numerical simulations show that our method can achieve decimeter-level accuracy in different environments for targets moving at different speeds, accelerations and decelerations, which outperforms the existing solutions.

6. REFERENCES

[1] M. G. Jules, "The global positioning system," *IEEE Transactions on Microwave theory and techniques*, vol. 50, no. 3, pp. 645–652, 2002.

[2] B. Wang, Q. Xu, C. Chen, F. Zhang, and K. J. R. Liu, "The promise of radio analytics: A future paradigm of wireless positioning, tracking, and sensing," *IEEE Signal Processing Magazine*, vol. 35, no. 3, pp. 59–80, May 2018.

[3] Z. Wu, Y. Han, Y. Chen, and K. J. R. Liu, "A time-reversal paradigm for indoor positioning system," *IEEE Transactions on Vehicular Technology*, vol. 64, no. 4, pp. 1331–1339, April 2015.

[4] C. Chen, Y. Chen, Y. Han, H. Lai, and K. J. R. Liu, "Achieving centimeter-accuracy indoor localization on WiFi platforms: A frequency hopping approach," *IEEE Internet of Things Journal*, vol. 4, no. 1, pp. 111–121, Feb 2017.

[5] J. Dai and H. C. So, "Sparse bayesian learning approach for outlier-resistant direction-of-arrival estimation," *IEEE Transactions on Signal Processing*, vol. 66, no. 3, pp. 744–756, 2018.

[6] X. Zeng, B. Chen, and M. Yang, "DOA estimation for low angle targets using time reversal in frequency domain model," in *2018 IEEE Radar Conference (RadarConf18)*, 2018, pp. 1323–1327.

[7] X. Zeng, M. Yang, B. Chen, and Y. Jin, "Estimation of direction of arrival by time reversal for low-angle targets," *IEEE Transactions on Aerospace and Electronic Systems*, vol. 54, no. 6, pp. 2675–2694, Dec 2018.

[8] A. Alessandrini, F. Mazzarella, and M. Vespe, "Estimated time of arrival using historical vessel tracking data," *IEEE Transactions on Intelligent Transportation Systems*, vol. 20, no. 1, pp. 7–15, 2019.

[9] H. C. So and L. Lin, "Linear least squares approach for accurate received signal strength based source localization," *IEEE Transactions on Signal Processing*, vol. 59, no. 8, pp. 4035–4040, 2011.

[10] X. Tian, S. Zhu, S. Xiong, B. Jiang, Y. Yang, and X. Wang, "Performance analysis of Wi-Fi indoor localization with channel state information," *IEEE Transactions on Mobile Computing*, vol. 18, no. 8, pp. 1870–1884, 2019.

[11] C. Wu, F. Zhang, B. Wang, and K. J. R. Liu, "Easitrack: Decimeter-level indoor tracking with graph-based particle filtering," *IEEE Internet of Things Journal*, vol. 7, no. 3, pp. 2397–2411, 2020.

[12] N. Garcia, H. Wymeersch, E. G. Larsson, A. M. Haimovich, and M. Coulon, "Direct localization for massive MIMO," *IEEE Transactions on Signal Processing*, vol. 65, no. 10, pp. 2475–2487, May 2017.

[13] X. Sun, C. Wu, X. Gao, and G. Y. Li, "Fingerprint-based localization for massive MIMO-OFDM system with deep convolutional neural networks," *IEEE Transactions on Vehicular Technology*, vol. 68, no. 11, pp. 10846–10857, 2019.

[14] X. Zeng, F. Zhang, B. Wang, and K. J. R. Liu, "Radio frequency based direction sensing using massive MIMO," *IEEE Access*, vol. 8, pp. 26827–26838, 2020.

[15] A. Taira, H. Iura, K. Nakagawa, S. Uchida, K. Ishioka, A. Okazaki, S. Suyama, T. Obara, Y. Okumura, and A. Okamura, "Performance evaluation of 44GHz band massive MIMObased on channel measurement," in *2015 IEEE Globecom Workshops (GC Wkshps)*, 2015, pp. 1–6.

[16] À. O. Martínez, J. Ø. Nielsen, E. De Carvalho, and P. Popovski, "An experimental study of massive MIMO properties in 5G scenarios," *IEEE Transactions on Antennas and Propagation*, vol. 66, no. 12, pp. 7206–7215, 2018.

[17] J. Chen, X. Yin, X. Cai, and S. Wang, "Measurement-based massive MIMO channel modeling for outdoor LoS and NLoS environments," *IEEE Access*, vol. 5, pp. 2126–2140, 2017.

[18] C. Xiao, Y. R. Zheng, and N. C. Beaulieu, "Novel sum-of-sinusoids simulation models for rayleigh and rician fading channels," *IEEE Transactions on Wireless Communications*, vol. 5, no. 12, pp. 3667–3679, December 2006.

[19] F. Zhang, C. Chen, B. Wang, H. Lai, Y. Han, and K. J. R. Liu, "Wiball: A time-reversal focusing ball method for decimeter-accuracy indoor tracking," *IEEE Internet of Things Journal*, vol. 5, no. 5, pp. 4031–4041, Oct 2018.

[20] R. Muller, D. A. Dupleich, C. Schneider, R. Herrmann, and R. S. Thoma, "Ultrawideband 3D mmwave channel sounding for 5G," in *2014 XXXIth URSI General Assembly and Scientific Symposium (URSI GASS)*, Aug 2014, pp. 1–4.

[21] Y. Azar, G. N. Wong, K. Wang, R. Mayzus, J. K. Schulz, H. Zhao, F. Gutierrez, D. Hwang, and T. S. Rappaport, "28 GHz propagation measurements for outdoor cellular communications using steerable beam antennas in new york city," in *2013 IEEE International Conference on Communications (ICC)*, June 2013, pp. 5143–5147.